ISSN (Print) 1226-1750
ISSN (Online) 2233-6656
Journal of Magnetics 23(2), 323-332 (2018) https://doi.org/10.4283/JMAG.2018.23.2.323

Diffusive Species in MHD Squeezed Fluid Flow Through non-Darcy Porous Medium with Viscous Dissipation and Joule Heating

S. Ahmad[1]*, M. Farooq[1], Aisha Anjum[1], M. Javed[1], M. Y. Malik[2,3], and A. S. Alshomrani[3]

[1]*Department of Mathematics and Statistics, Riphah International University, Islamabad 44000, Pakistan*
[2]*Department of Mathematics, Quaid-I-Azam University, Islamabad 44000, Pakistan*
[3]*Department of Mathematics, Faculty of Science, King Abdulaziz University, Jeddah 21589, Saudi Arabia*

(Received 7 January 2018, Received in final form 15 April 2018, Accepted 26 April 2018)

This article focuses the flow through non-Darcy porous medium. The flow is due to the squeezing phenomenon. The magneto viscous fluid is accounted. Formulation of the flow problem is interpreted the salient features of Ohmic heating (Joule heating), viscous dissipation and auto-catalyst and reactants (i.e. homogeneous-heterogeneous reactions). A whole analysis is carried out with different diffusion coefficients for both auto-catalyst and reactants. It is also desired to observe the dependence of convective surface condition on flow regime in heat transport process. The resulting non-linear partial differential equations are found to be governing by dimensionless ordinary differential equations with the implementation of similarity solutions. A homotopic procedure based on an iterative scheme is utilized for the solutions of the flow problem. Flow velocity, fluid temperature and concentration are addressed via graphs for different values of geometrical and rheological parameters of considered flow problem. Moreover, skin friction co-efficient and Nusselt number are sketched and discussed graphically. The analysis reveals that higher values of mass diffusion ratio parameter result reduction in concentration of specie *B* whereas concentration of specie *A* enhances for higher mass diffusion ratio parameter.

Keywords : squeezing flow, non-Darcy porous medium, convective boundary condition, joule heating, homogeneous-heterogeneous reactions, viscous dissipation

1. Introduction

Dissipation effects as an energy source are played a vital role in the heat transport phenomenon. Joule heating (Ohmic heating) and viscous dissipation get more significance when plates are heating or cooling. The perceptible fact of the heat transport phenomenon occurs in the processes of power generation systems, cooling of metallic sheets or electronic chips, liquid metal fluids, cooling of nuclear reactors. Moreover, the Joule heating (Ohmic heating) process generates heat due to the resistance arises by passage of electric current through the material. The Joule heating has valuable as well as adverse influence on the system. A few systems that exploit the Joule heating effects include thermistors and soldering irons, di-electrophoretic trapping, hot plate, PCR reactors, micro-valves for fluid control, electric heaters and stoves, bio-particles manipulation in dilute medium, electric fuses etc. On the other hand, inadmissible heat produces in some processes which can melts or debase the machinery parts, may create denaturation of biological samples (proteins, DNA etc.), bubble formation, malfunctioning of chip systems etc. Hayat *et al.* [1] portrayed the impact of heat transfer characterized by Newtonian and Joule heating effects on Williamson fluid flow over shrinking surface. The properties of the magneto-hydrodynamics in Sisko nano-fluid flow over stretched cylinder with Ohmic heating and viscous dissipation are examined by Hussain *et al.* [2]. Sulochana *et al.* [3] disclosed the influence of the Joule heating on MHD radiative flow of nano-fluid along the continual moving needle. The characteristics of the Joule heating in the convectively heated MHD Maxwell fluid flow through the wall jet are portrayed by Zaidi and Mohyuddin [4]. The behavior of the Joule heating in the radiative peristalsis flow in a curved channel is constructed by Hayat *et al.* [5]. Shagaiy *et al.*

*Corresponding author: Tel: +923335377399
e-mail: shakeel_oiiui@hotmail.com

[6] addressed the heat transport phenomenon featured via dissipation effects in MHD radiative nano-fluid along with double stratification. Das *et al.* [7] exhibited the mixed convective slip flow of the MHD viscous fluid over a porous plate with dissipation effects. Khan *et al.* [8] disclosed the behavior of nano-fluid flow generated via slandering surface with non-linear radiative effect. Khan *et al.* [9] explored the dissipation effects on nano-fluid flow induced by rotating disk.

Chemically reactive processes featured via homogeneous-heterogeneous reactions which behave differently in the presence or absence of the catalyst. In industrial processes, catalysts are usually observed to increase the effectiveness of the chemical reactions. The constitutive relationship among the homogeneous-heterogeneous reactions is specifically elaborated. Chemical reaction is effectively important in the manufacturing of ceramics, food processing, polymer production, metallurgy and hydrometallurgical industry, crops damage via freezing and chemical processing equipment design etc. Markin [10] explored the features of the auto-catalyst and reactants in the concept of boundary layer flow theory for isothermal model. Hayat *et al.* [11] disclosed the melting phenomenon in flow of stagnant Jeffrey fluid with homogeneous and heterogeneous reactions. Khan *et al.* [12] explained the variation of the heat and mass transport featured via heat generation (or absorption) on Maxwell fluid flow with homogeneous-heterogeneous reactions. Significance of dissipation effects on hydro-magnetic flow of stagnant Casson liquid for the isothermal model is demonstrated by Khan *et al.* [13]. Xu [14] presented the isothermal model for stagnation flow of the heated fluid through a plane surface. Hayat *et al.* [15] exhibited the effect of homogeneous-heterogeneous model on a convectively heated nano-fluid flow via porous medium. Farooq *et al.* [16] explored the properties of the homogeneous-heterogeneous model in the flow over a Riga plate of variable thickness with melting condition. Raju *et al.* [17] elaborated the behavior of induced magnetic effects on the flow of stagnant Casson fluid with homogeneous-heterogeneous reactions. Few recent contributions in the area of the homogeneous-heterogeneous reactions are made in the refs. [18, 19].

A close scrutiny of the scientific literature aimed that no studies have been appeared in the communications where the squeezing flow analysis is accounted under the Darcy Forchheimer theory for the hydro-magnetic fluid with the homogeneous-heterogeneous reactions. The objective of this analysis is to fill such void. Therefore the present attempt is described the MHD squeezing flow through a Forchheimer porous media. The heat transfer process involves convective boundary condition and dissipation effects (Joule heating and viscous dissipation). The homogeneous-heterogeneous reactions are utilized to explore the mass transport phenomenon. The convergent series solutions of the problem are evaluated by homotopic technique [20-28]. The contributions of different embedding parameters are plotted and addressed. Skin friction co-efficient and Nusselt number are exhibited through graphical data.

2. Mathematical Modeling

Consider the unsteady squeezed viscous fluid flow between parallel two plates. The incompressible fluid saturates the porous medium featuring the Darcy-Forchheimer model. The fluid is the electrically conducting and strength $B_0/\sqrt{(1-\gamma t)}$ of the magnetic field is applied along the y-direction. The lower plate is fixed at $y = 0$ and the upper plate at $h(t) = \sqrt{\nu(1-\gamma t)/a}$. Here $h(t)$ represents the width between the plates and γ denotes the dimensional constant. Further, upper plate is squeezed towards the immovable lower stretching plate satisfying convective heat condition. The flow phenomenon is studied in the Cartesian co-ordinate system (x, y). The direction of x and y co-ordinates are as shown in Fig. 1.

The heat transfer phenomenon is explored with the Joule heating and viscous dissipation. T, a and b represent the temperature and the concentration respectively. The convective heating process provides the temperature T_f and T_h denotes the upper plate temperature. Flow analysis is also carried out through a homogeneous-heterogeneous reactions of species A and B. Basic model of the homogeneous and heterogeneous reactions are initiated by Merkin [10] i.e.

$$A + B \rightarrow 3B\,,\ rate = k_c ab^2, \tag{1}$$

which represents the isothermal cubic autocatalysis reaction while first-order and isothermal reaction on the catalyst surface is given by

$$A \rightarrow B\,,\ rate = k_s a. \tag{2}$$

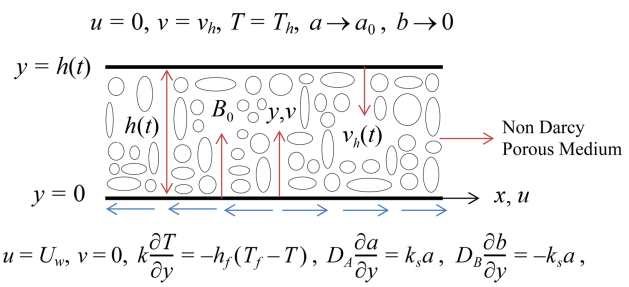

Fig. 1. (Color online) Schematic of flow situation.

where k_c and k_s denote the constant rate while a and b indicate the concentration of chemical species A and B respectively.

The conservative flow laws under consideration take the form

$$\frac{\partial u}{\partial x}+\frac{\partial v}{\partial y}=0\,, \tag{3}$$

$$\frac{\partial u}{\partial t}+u\frac{\partial u}{\partial x}+v\frac{\partial u}{\partial y}=-\frac{1}{\rho}\frac{\partial p}{\partial x}+\nu\left(\frac{\partial^2 u}{\partial x^2}+\frac{\partial^2 u}{\partial y^2}\right)$$
$$-\frac{\sigma B_0^2}{\rho(1-\gamma t)}u-\frac{\nu\phi^*}{k^*}u-\frac{C_b\phi^*}{\sqrt{k^*}}u^2\,, \tag{4}$$

$$\frac{\partial v}{\partial t}+u\frac{\partial v}{\partial x}+v\frac{\partial v}{\partial y}=-\frac{1}{\rho}\frac{\partial p}{\partial y}+\nu\left(\frac{\partial^2 v}{\partial x^2}+\frac{\partial^2 v}{\partial y^2}\right)$$
$$-\frac{\nu\phi^*}{k^*}v-\frac{C_b\phi^*}{\sqrt{k^*}}v^2\,, \tag{5}$$

$$\frac{\partial T}{\partial t}+u\frac{\partial T}{\partial x}+v\frac{\partial T}{\partial y}=\frac{k}{\rho C_p}\left(\frac{\partial^2 T}{\partial x^2}+\frac{\partial^2 T}{\partial y^2}\right)$$
$$+\frac{\mu}{\rho C_p}\left(4\left(\frac{\partial u}{\partial x}\right)^2+\left(\frac{\partial u}{\partial y}+\frac{\partial v}{\partial x}\right)^2\right)+\frac{\sigma B_0^2}{\rho C_p(1-\gamma t)}u^2\,, \tag{6}$$

$$\frac{\partial a}{\partial t}+u\frac{\partial a}{\partial x}+v\frac{\partial a}{\partial y}=D_A\left(\frac{\partial^2 a}{\partial x^2}+\frac{\partial^2 a}{\partial y^2}\right)-k_c ab^2\,, \tag{7}$$

$$\frac{\partial b}{\partial t}+u\frac{\partial b}{\partial x}+v\frac{\partial b}{\partial y}=D_B\left(\frac{\partial^2 b}{\partial x^2}+\frac{\partial^2 b}{\partial y^2}\right)+k_c ab^2\,, \tag{8}$$

Here u and v represent the velocity components along x and y direction respectively. p is the pressure, ν denotes the kinematics viscosity, σ denotes the electric conductivity, μ denotes the absolute viscosity, B_0 is the magnetic field, ρ represents the fluid density, ϕ^* and k^* denote the porosity and the permeability of the porous medium respectively, $C_b^* = (C_b/x)$ denotes the drag co-efficient, T is the fluid temperature, k is the co-efficient of thermal conductivity, C_p represents the specific heat capacity, D_A and D_B are the diffusion co-efficient of species A and B respectively.

The boundary conditions are as follow

$$u=U_w=\frac{dx}{1-\gamma t}\,,\ v=0,\ k\frac{\partial T}{\partial y}=-h_f[T_f-T]\,,$$
$$D_A\frac{\partial a}{\partial y}=k_s a\,,\ D_B\frac{\partial b}{\partial y}=-k_s a\ \text{ at } y=0,$$
$$u=0,\ v=v_h=\frac{dh}{dt}=-\frac{\gamma}{2}\sqrt{\frac{\nu}{d(1-\gamma t)}}\,,\ T=T_h,\ a\to a_0\,,$$
$$b\to 0\ \text{ at } y=h(t). \tag{9}$$

Here U_w represents the stretching velocity, d represents the dimensional constant, h_f represents the convective heat transfer coefficient, T_f represents the convective fluid temperature, T_h represents the temperature of the upper plate and a_0 represents the constant concentration at the upper wall.

Selecting the suitable similarity variables of the form

$$\eta=\frac{y}{h(t)}\,,\ \Psi=\sqrt{\frac{d\nu}{1-\gamma t}}xf(\eta)\,,\ u=U_w f'(\eta)\,,$$
$$v=-\sqrt{\frac{d\nu}{1-\gamma t}}f(\eta)\,,\ \theta(\eta)=\frac{T-T_h}{T_f-T_h}\,,\ \phi(\eta)=\frac{a}{a_0}\,,$$
$$g(\eta)=\frac{b}{a_0}\,. \tag{10}$$

Here Ψ represents the stream function, η represents the similarity variable, $f(\eta)$ represents the non-dimensional variable, $\theta(\eta)$, $\phi(\eta)$ and $g(\eta)$ represent the dimensionless temperature and dimensionless concentration of species A and B respectively.

Continuity equation is verified identically. Eliminating pressure term from equations (4)-(5) and in view of equation (10), we obtain the constitutive flow equations as below

$$f^{(iv)}+ff'''-f'f''-\frac{S_q}{2}(3f''+\eta f''')-M^2f''$$
$$-Da^{-1}f''-2\alpha_1 f'f''=0\,, \tag{11}$$

$$\theta''+Pr\left(f\theta'-\frac{1}{2}S_q\eta\theta'\right)$$
$$+PrEc((f'')^2+4\delta^2(f')^2+M^2(f')^2)=0\,, \tag{12}$$

$$\phi''+Sc\left(f\phi'-\frac{1}{2}S_q\eta\phi'\right)-Sck_1\phi g^2=0\,, \tag{13}$$

$$\delta_1 g''+Sc\left(fg'-\frac{1}{2}S_q\eta g'\right)+Sck_1\phi g^2=0\,, \tag{14}$$

with subjected boundary conditions

$$f(0)=0, f'(0)=1, f'(1)=0,\ f(1)=\frac{S_q}{2}\,,$$
$$\theta'(0)=-B_i(1-\theta(0))\ ,\ \theta(1)=0,\ \phi'(0)=k_2\phi(0)\,,$$
$$\phi(1)=1\,,\ \delta_1 g'(0)=-k_2\phi(0)\,,\ g(1)=0, \tag{15}$$

where squeezing parameter S_q, magnetic parameter M^2, inverse Darcy number Da^{-1}, local inertia coefficient parameter α_1, Prandtl number Pr, Eckert number Ec, length parameter δ, Biot number B_i, ratio of mass diffusion coefficient δ_1, Schmidt number Sc, strength of homogeneous reaction parameter k_1 and strength of heterogeneous reaction parameter k_2 are given by

$$S_q = \frac{\gamma}{d},\ Da^{-1} = \frac{\nu\phi^*(1-\gamma t)}{k^* d},\ M^2 = \frac{\sigma B_0^2}{\rho d},\ \alpha_1 = \frac{C_b^*}{\sqrt{k^*}}\phi^*,$$

$$Pr = \frac{\mu C_p}{k},\ Ec = \frac{d^2x^2}{C_p(1-\gamma t)^2(T_f - T_h)},\ \delta = \frac{\sqrt{\nu(1-\gamma t)}}{x\sqrt{d}},$$

$$B_t = \frac{h_f\sqrt{\nu(1-\gamma t)}}{\sqrt{d}},\ \delta_1 = \frac{D_B}{D_A},\ Sc = \frac{\nu}{D_A},$$

$$k_1 = \frac{k_c d^2(1-\gamma t)}{d},\ k_2 = \frac{k_s\sqrt{\nu(1-\gamma t)}}{\sqrt{d}}. \tag{16}$$

It is observed that for $S_q < 0$, the plates are moving away and for $S_q > 0$, the plates are moving towards each other respectively.

Defining local skin friction co-efficient Cf_x and local Nusselt number Nu_x as

$$Cf_x = \frac{\mu(\tau_{xy})|_{y=h(t)}}{\rho U_w^2},\ Nu_x = \frac{-xk\left(\frac{\partial T}{\partial y}\right)\Big|_{y=h(t)}}{k(T_f - T_h)}, \tag{17}$$

In view of the equation (10), the equation (17) takes the form

$$(Re_x)^{\frac{1}{2}} Cf_x = f''(1),\ (Re_x)^{\frac{-1}{2}} Nu_x = -\theta'(1). \tag{18}$$

Where $Re_x = U_w x/\nu$ represents the local Reynolds number.

3. Homotopy Solutions

Consider the initial guesses (f_0, θ_0, ϕ_0, g_0) and linear operators $\mathcal{L}_f$, $\mathcal{L}_\theta$, $\mathcal{L}_\phi$, $\mathcal{L}_g$ for homotopic procedure as

$$f_0(\eta) = \frac{1}{2}(2\eta - 4\eta^2 + 3S_q\eta^2 + 2\eta^3 - 32\eta^3), \tag{19}$$

$$\theta_0(\eta) = \frac{B_t}{1+B_t}(1-\eta), \tag{20}$$

$$\phi_0(\eta) = \frac{1}{1+k_2}(1+k_2\eta),\ g_0(\eta) = \frac{k_2}{\delta_1(1+k_2)}(1-\eta), \tag{21}$$

$$\mathcal{L}_f = f'''',\ \mathcal{L}_\theta = \theta'',\ \mathcal{L}_\phi = \phi'',\ \mathcal{L}_g = g'', \tag{22}$$

with

$$\mathcal{L}_f(C_1 + C_2\eta + C_3\eta^2 + C_4\eta^4) = 0,\ \mathcal{L}_\theta(C_5 + C_6\eta) = 0,$$
$$\mathcal{L}_\phi(C_7 + C_8\eta) = 0,\ \mathcal{L}_g(C_9 + C_{10}\eta) = 0. \tag{23}$$

where $C_i (i = 1-10)$ are arbitrary constants.

3.1. Zeroth-order problems

Here,

$$(1-q)\mathcal{L}_f[\breve{f}(\eta;q) - f_0(\eta)] = p\hbar_f N_f[\breve{f}(\eta;q)],$$
$$\breve{f}(0;q) = 0,\ \breve{f}'(0;q) = 1,\ \breve{f}(1;q) = \frac{S_q}{2},$$
$$\breve{f}'(1;q) = 0, \tag{24}$$

$$(1-q)\mathcal{L}_\theta[\breve{\theta}(\eta;q) - \theta_0(\eta)] = p\hbar_\theta N_\theta[\breve{\theta}(\eta;q)],$$
$$\breve{\theta}(0;q) = -B_t(1-\breve{\theta}(0;q)),\ \breve{\theta}(1;q) = 0, \tag{25}$$

$$(1-q)\mathcal{L}_\phi[\breve{\phi}(\eta;q) - \phi_0(\eta)] = p\hbar_\phi N_\phi[\breve{\phi}(\eta;q)],$$
$$\breve{\phi}(0;q) = k_2\breve{\phi}(0;q),\ \breve{\phi}(1;q) = 1, \tag{26}$$

$$(1-q)\mathcal{L}_g[\breve{g}(\eta;q) - g_0(\eta)] = p\hbar_g N_g[\breve{g}(\eta;q)],$$
$$\delta_1\breve{g}(0;q) = -k_2\breve{\phi}(0;q),\ \breve{g}(1;q) = 0. \tag{27}$$

Defining non-linear operators as

$$N_f[\breve{f}(\eta;q)] = \frac{\partial^4\breve{f}(\eta;q)}{\partial\eta^4} + \breve{f}(\eta;q)\frac{\partial^3\breve{f}(\eta;q)}{\partial\eta^3}$$
$$-\frac{\partial\breve{f}(\eta;q)}{\partial\eta}\frac{\partial^2\breve{f}(\eta;q)}{\partial\eta^2} - \frac{S_q}{2}\left(3\frac{\partial^2\breve{f}(\eta;q)}{\partial\eta^2} + \eta\frac{\partial^2\breve{f}(\eta;q)}{\partial\eta^3}\right)$$
$$-M^2\frac{\partial^2\breve{f}(\eta;q)}{\partial\eta^2} - Da^{-1}\frac{\partial^2\breve{f}(\eta;q)}{\partial\eta^2}$$
$$-2\alpha_1\frac{\partial\breve{f}(\eta;q)}{\partial\eta}\frac{\partial^2\breve{f}(\eta;q)}{\partial\eta^2}, \tag{28}$$

$$N_\theta[\breve{\theta}(\eta;q)] = \frac{\partial^2\breve{\theta}(\eta;q)}{\partial\eta^2}$$
$$+Pr\left(\breve{f}(\eta;q)\frac{\partial\breve{\theta}(\eta;q)}{\partial\eta} - \frac{1}{2}S_q\eta\frac{\partial\breve{\theta}(\eta;q)}{\partial\eta}\right) \tag{29}$$
$$+PrEc\left(\left(\frac{\partial^2\breve{f}(\eta;q)}{\partial\eta^2}\right)^2 + 4\delta^2\left(\frac{\partial\breve{f}(\eta;q)}{\partial\eta}\right)^2 + M^2\left(\frac{\partial\breve{f}(\eta;q)}{\partial\eta}\right)^2\right),$$

$$N_\phi[\breve{\phi}(\eta;q)] = \frac{\partial^2\breve{\phi}(\eta;q)}{\partial\eta^2}$$
$$+Sc\left(f(\eta;q)\frac{\partial\breve{\phi}(\eta;q)}{\partial\eta} - \frac{1}{2}S_q\eta\frac{\partial\breve{\phi}(\eta;q)}{\partial\eta}\right)$$
$$-Sck_1\breve{\phi}(\eta;q)(\breve{g}(\eta;q))^2 \tag{30}$$

$$N_g[\breve{g}(\eta;q)] = \frac{\partial^2\breve{g}(\eta;q)}{\partial\eta^2}$$
$$+\frac{Sc}{\delta_1}\left(f(\eta;q)\frac{\partial\breve{g}(\eta;q)}{\partial\eta} - \frac{1}{2}S_q\eta\frac{\partial\breve{g}(\eta;q)}{\partial\eta}\right)$$
$$+\frac{Sc}{\delta_1}k_1\breve{\phi}(\eta;q)(\breve{g}(\eta;q))^2 \tag{31}$$

where $q \in [0,1]$ is embedding parameter and auxiliary non-zero parameters are $\hbar_f$, $\hbar_\theta$, $\hbar_\phi$ and $\hbar_g$.

3.2. mth-order problems

Here,

$$\mathcal{L}_f[f_m(\eta) - \chi_m f_{m-1}(\eta)] = \hbar_f R_m^f(\eta),$$
$$f_m(0) = 0,\ f_m'(0) = 0,\ f_m(1) = 0,\ f_m'(1) = 0, \tag{32}$$

$$\mathcal{L}_\theta[\theta_m(\eta) - \chi_m \theta_{m-1}(\eta)] = \hbar_\theta R_m^\theta(\eta),$$
$$\theta_m'(0) - B_t\theta(0) = 0,\ \theta_m(1) = 0, \tag{33}$$

$$\mathcal{L}_\phi[\phi_m(\eta) - \chi_m \phi_{m-1}(\eta)] = \hbar_f R_m^\phi(\eta),$$
$$\phi_m'(0) - k_2\phi_m(0) = 0,\ \phi_m(1) = 0, \tag{34}$$

$$\mathcal{L}_g[g_m(\eta) - \chi_m g_{m-1}(\eta)] = \hbar_g R_m^g(\eta),$$
$$g_m'(0) + \frac{k_2}{\delta_1}\phi_m(0) = 0,\ g_m(1) = 0, \tag{35}$$

Defining non-linear operators as follows

$$R_m^f(\eta) = f_{m-1}^{(iv)} + \sum_{k=0}^{m-1} f_{m-1-k} f_k''' - \sum_{k=0}^{m-1} f_{m-1-k}' f_k''$$
$$- \frac{S_q}{2}(3f_{m-1}'' + \eta f_{m-1}''')$$
$$-M^2 f_{m-1}'' - Da^{-1} f_{m-1}'' - 2\alpha_1 \sum_{k=0}^{m-1} f_{m-1-k}' f_k'', \tag{36}$$

$$R_m^\theta(\eta) = \theta_{m-1}'' + Pr\left(\sum_{k=0}^{m-1} f_{m-1-k}\theta_k' + \frac{1}{2}S_q\eta\theta_{m-1}'\right)$$
$$+ PrEc\left(\sum_{k=0}^{m-1} f_{m-1-k}'' f_k'' + 4\delta^2 \sum_{k=0}^{m-1} f_{m-1-k}' f_k'\right.$$
$$\left. + M^2 \sum_{k=0}^{m-1} f_{m-1-k}' f_k'\right), \tag{37}$$

$$R_m^\phi(\eta) = \phi_{m-1}'' + Sc\left(\sum_{k=0}^{m-1} f_{m-1-k}\phi_k' - \frac{1}{2}S_q\eta\phi_{m-1}'\right)$$
$$- Sck_1 \sum_{k=0}^{m-1} \phi_{m-1-k} \sum_{p=0}^{k} g_{k-p} g_p\Bigg), \tag{38}$$

$$R_m^g(\eta) = g_{m-1}'' + \frac{Sc}{\delta_1}\left(\sum_{k=0}^{m-1} f_{m-1-k} g_k' - \frac{1}{2}S_q\eta g_{m-1}'\right)$$
$$+ \frac{Sc}{\delta_1}k_1 \sum_{k=0}^{m-1} \phi_{m-1-k} \sum_{p=0}^{k} g_{k-p} g_p\Bigg), \tag{39}$$

$$\chi_m = \begin{cases} 0, & m \le 1 \\ 1, & m > 1 \end{cases}, \tag{40}$$

for $q = 0$ and $q = 1$, we can write

$$\breve{f}(\eta;0) = f_0(\eta),\ \breve{f}(\eta;1) = f(\eta),$$
$$\breve{\theta}(\eta;0) = \theta_0(\eta),\ \breve{\theta}(\eta;1) = \theta(\eta),$$
$$\breve{\phi}(\eta;0) = \phi_0(\eta),\ \breve{\phi}(\eta;1) = \phi(\eta),$$
$$\breve{g}(\eta;0) = g_0(\eta),\ \breve{g}(\eta;1) = g(\eta), \tag{41}$$

and with the variation of q from 0 to 1, $\breve{f}(\eta;q)$, $\breve{\theta}(\eta;q)$, $\breve{\phi}(\eta;q)$ and $\breve{g}(\eta;q)$ vary from the initial solutions $f_0(\eta)$, $\theta_0(\eta)$, $\phi_0(\eta)$ and and $g_0(\eta)$ to the final solutions $f(\eta)$, $\theta(\eta)$, $\phi(\eta)$ and $g(\eta)$ respectively. By Taylor series, we have

$$\breve{f}(\eta;q) = f_0(\eta) + \sum_{m=1}^{\infty} f_m(\eta)q^m,\ f_m(\eta) = \frac{1}{m!}\frac{\partial^m \breve{f}(\eta;q)}{\partial q^m}\bigg|_{q=0},$$
$$\breve{\theta}(\eta;q) = \theta_0(\eta) + \sum_{m=1}^{\infty} \theta_m(\eta)q^m,\ \theta_m(\eta) = \frac{1}{m!}\frac{\partial^m \breve{\theta}(\eta;q)}{\partial q^m}\bigg|_{q=0},$$
$$\breve{\phi}(\eta;q) = \phi_0(\eta) + \sum_{m=1}^{\infty} \phi_m(\eta)q^m,\ \phi_m(\eta) = \frac{1}{m!}\frac{\partial^m \breve{\phi}(\eta;q)}{\partial q^m}\bigg|_{q=0},$$
$$\breve{g}(\eta;q) = g_0(\eta) + \sum_{m=1}^{\infty} g_m(\eta)q^m,\ g_m(\eta) = \frac{1}{m!}\frac{\partial^m \breve{g}(\eta;q)}{\partial q^m}\bigg|_{q=0}, \tag{42}$$

choose suitable value for auxiliary parameter that the series (42) converge at $q = 1$ i.e.

$$f(\eta) = f_0(\eta) + \sum_{m=1}^{\infty} f_m(\eta),$$
$$\theta(\eta) = \theta_0(\eta) + \sum_{m=1}^{\infty} \theta_m(\eta),$$
$$\phi(\eta) = \phi_0(\eta) + \sum_{m=1}^{\infty} \phi_m(\eta),$$
$$g(\eta) = g_0(\eta) + \sum_{m=1}^{\infty} g_m(\eta), \tag{43}$$

f_m, θ_m, ϕ_m and g_m represent general solutions for equations (32-35) in the form of special solutions (f_m^*, θ_m^*, ϕ_m^*, g_m^*) are given by

$$f_m(\eta) = f_m^*(\eta) + C_1 + C_2\eta + C_3\eta^2 + C_4\eta^3,$$
$$\theta_m(\eta) = \theta_m^*(\eta) + C_5 + C_6\eta,$$
$$\phi_m(\eta) = \phi_m^*(\eta) + C_7 + C_8\eta,$$
$$g_m(\eta) = g_m^*(\eta) + C_9 + C_{10}\eta. \tag{44}$$

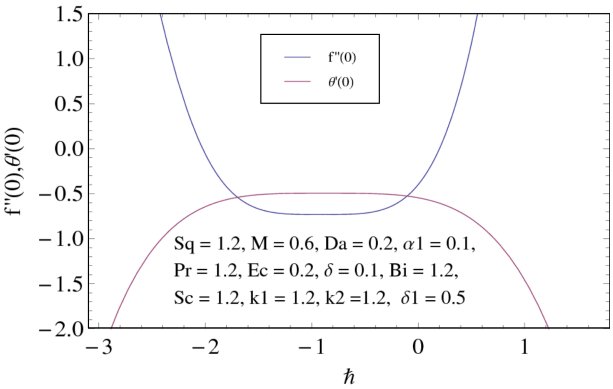

(a)

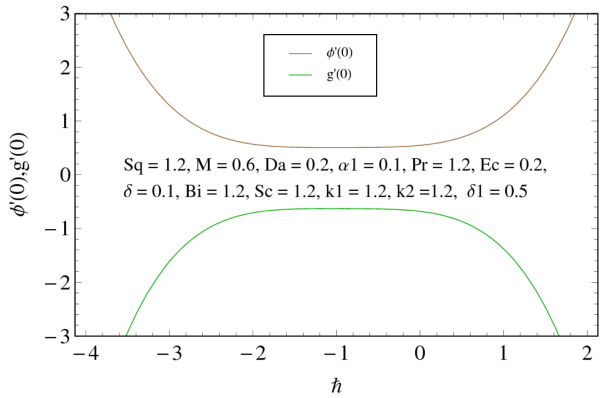

(b)

Fig. 2. (Color online) (a) Convergence region for $f(\eta)$ and $\theta(\eta)$. (b) Convergence region for $\phi(\eta)$ and $g(\eta)$.

3.3. Convergence of problem

In order to develop the iterative solutions of the flow problem, our purpose is to determine the convergence region to ensure the iterative solutions incorporated in equation (44) are convergent. Convergence region of the flow problem depends upon the auxiliary parameters $\hbar_f$, $\hbar_\theta$, $\hbar_\phi$ and $\hbar_g$ for which $\hbar$-curves are sketched in Fig. 2. It is found that allowable ranges for the parameters $\hbar_f$, $\hbar_\theta$, $\hbar_\phi$ and $\hbar_g$ are $-1.4 \le \hbar_f \le -0.5$, $-1.5 \le \hbar_\theta \le -0.2$, $-1.8 \le \hbar_\phi \le -0.3$ and $-1.7 \le \hbar_\phi \le -0.6$

4. Discussion

This segment is graphed to elaborate the behavior of the flow parameters on the velocity components, temperature and the fluid concentration. Further, the skin friction and Nusselt number are also examined via these parameters.

4.1. Dimensionless velocity distributions

The variation of the squeezing parameter S_q on the velocity field is illustrated in Figs. 3, 4. It is evident that the velocity components grow up for larger values of

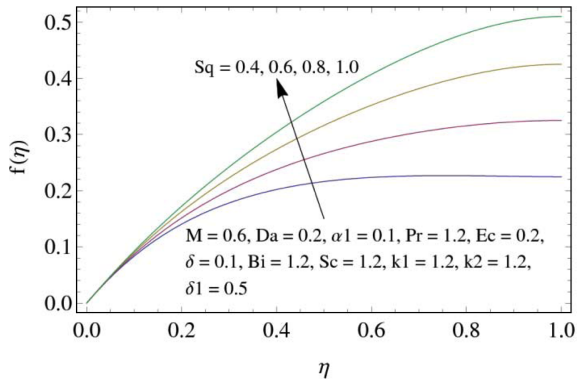

Fig. 3. (Color online) Variation of S_q on $f(\eta)$.

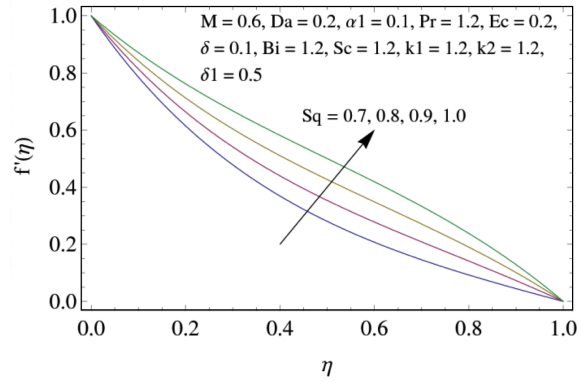

Fig. 4. (Color online) Variation of S_q on $f'(\eta)$.

squeezing parameter. Physically, fluid deformed rapidly due to the squeezing force exerted by walls. Hence velocity components (i.e. horizontal and vertical velocities) increase. Further the velocity profile increases for the higher values of η. The velocity field is smaller at the lower surface while maximum at the upper plate. The influence of the magnetic parameter (M) on the horizontal velocity field is indicated in Fig. 5. It is reflected that horizontal velocity diminishes for increasing magnetic parameter near the lower plate whereas it dominants towards the upper plate.

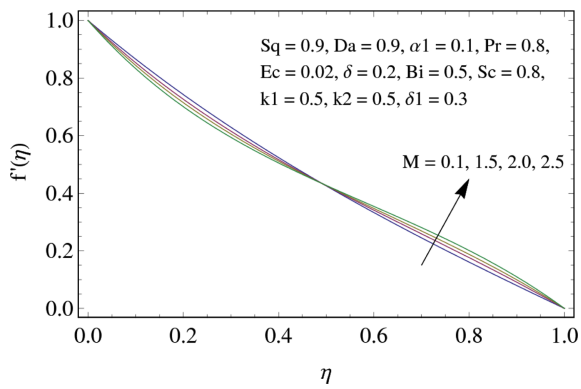

Fig. 5. (Color online) Variation of M on $f'(\eta)$.

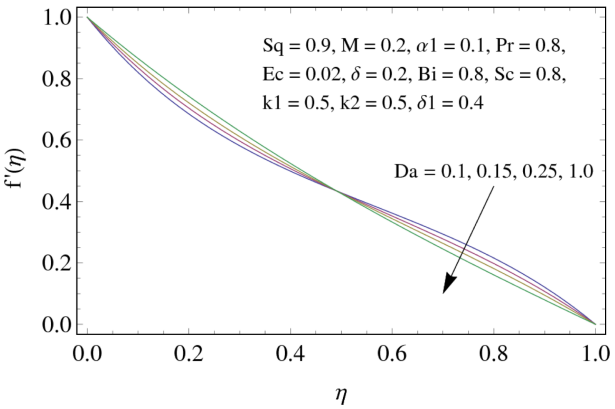

Fig. 6. (Color online) Variation of Da on $f'(\eta)$.

In fact, the wall parallel Lorentz force (resistive force) is stronger near the wall as compared to the central region of the flow. So that decrease in the flow velocity in the region bounded by walls will balance the increase in the velocity field within the central region give rise to the cross flow behavior which is expected in MHD flow. Fig. 6 presents that an increment in the Darcy number Da causes horizontal velocity to dominate immediate to the lower plate i.e. in the region $0 \le \eta \le 0.5$ while reduction is observed towards the upper plate $0.5 \le \eta \le 1.0$. Physically, parameter Da represents the resistance to the flow which decreases the fluid velocity towards the upper wall. Fig. 7 exhibits the variation in horizontal velocity field corresponds to the local inertia coefficient parameter α_1. It is seen that higher local inertia coefficient parameter decays the horizontal velocity component in the region $0 \le \eta \le 0.5$ due to the increase in porosity results reduction in pore velocity while opposite behavior is featured in the region $0.5 \le \eta \le 1$. Fig. 8 indicates the variation of x and η on horizontal velocity component u. It is observed that an increment in x causes to enhance the stretching velocity at the left plane while it is minimum at the right plane of the channel.

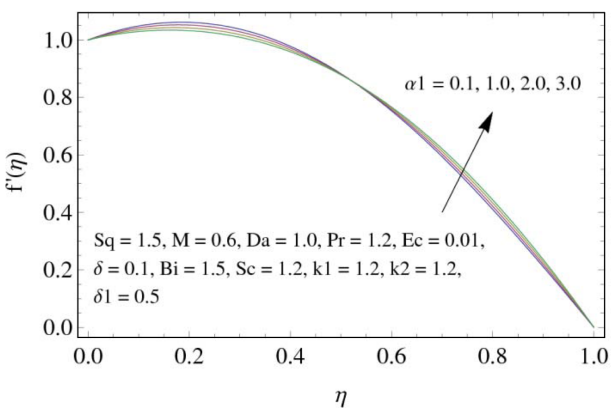

Fig. 7. (Color online) Variation of α_1 on $f'(\eta)$.

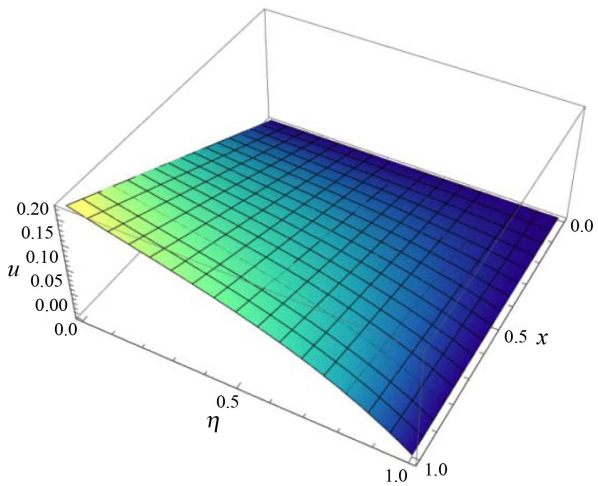

Fig. 8. (Color online) 3D plot of u with x & η.

4.2. Temperature distribution

Figure 9 examines the variation of the squeezing parameter (S_q) on temperature field. It describes the reduction in the temperature for the greater squeezing parameter. Here when plates get closer, the temperature is relatively large, increasing (S_q) decays kinematic viscosity and as a results temperature profile decreases. Fig. 10 discloses the enhancing behavior of the temperature with magnetic parameter M. It is noticed that temperature field dominant for growing M. The physics behind is that the fluid resistance increases due to the resistive forces (Lorentz forces) because of an increment in the applied magnetic field which leads to enlargement in the temperature. Fig. 11 represents the impact of Eckert number (Ec) on the fluid temperature. It is found that the temperature field hike for higher Eckert number. Physically, larger Eckert number increases the kinetic energy of the fluid particles which strengthen the temperature

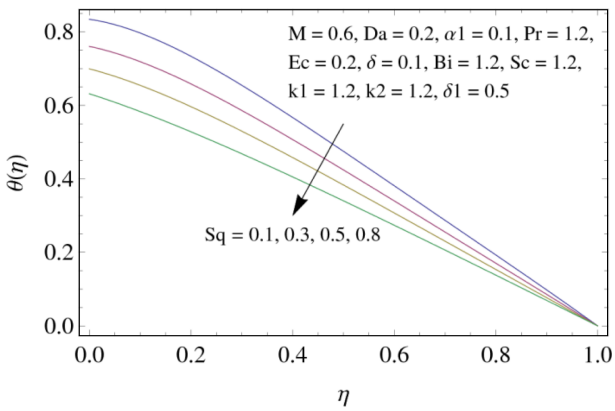

Fig. 9. (Color online) Variation of S_q on $\theta(\eta)$.

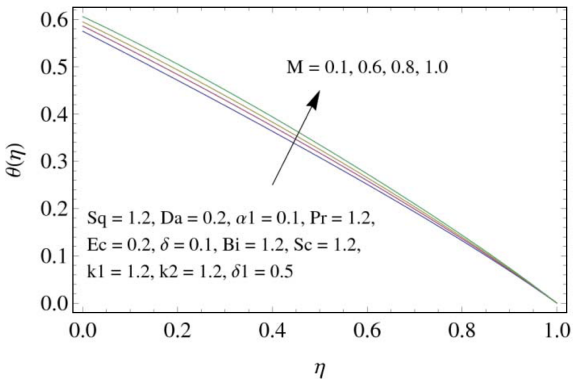

Fig. 10. (Color online) Variation of M on $\theta(\eta)$.

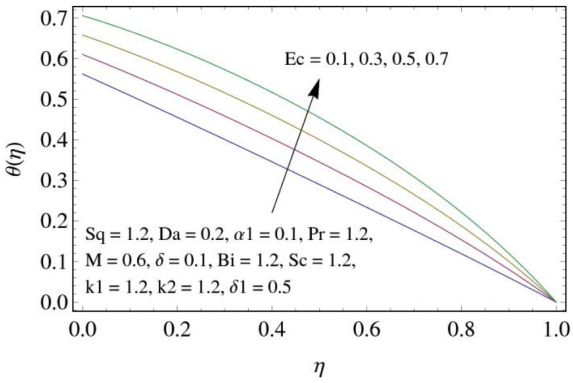

Fig. 11. (Color online) Variation of Ec on $\theta(\eta)$.

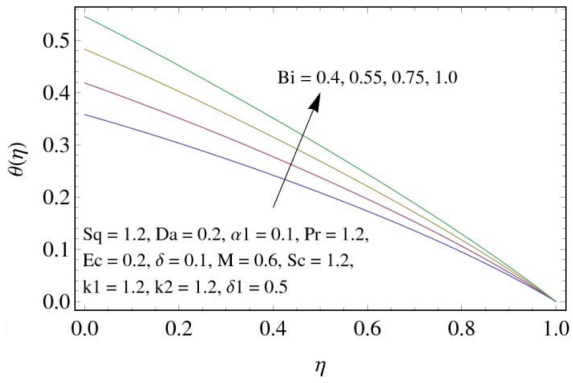

Fig. 12. (Color online) Variation of B_i on $\theta(\eta)$.

distribution. The features of Biot number (B_i) on the temperature field is reflected in Fig. 12. An enlargement in the Biot number leads to strengthen the temperature profile. Physically, it justifies that for larger (B_i) the convective heating at the lower plate increases due to which the transfer of the heat to the fluid increases and as a result temperature profile grows up.

4.3. Concentration distribution

The variation in the concentration distribution for Schmidt number Sc is suggested in Fig. 13. It is evident

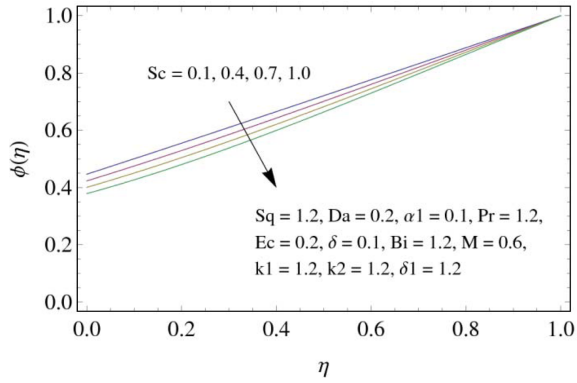

Fig. 13. (Color online) Variation of Sc on $\phi(\eta)$.

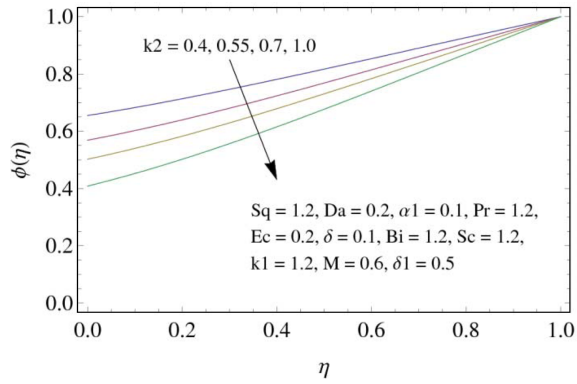

Fig. 14. (Color online) Variation of k_2 on $\phi(\eta)$.

that an increment in the Schmidt number results reduction in concentration profile (a) of specie A. As the Schmidt number increases, the mass diffusivity decays which results away movement of the particles and consequently concentration decays. Fig. 14 discloses the variation of strength of the heterogeneous reaction parameter k_2 versus concentration distribution. Enlarge k_2 diminishes the concentration. In fact, k_2 relates inversely to the diffusion coefficient so that the reaction rate grows up for weaker diffusion rate. Hence specie's concentration decays. Fig.

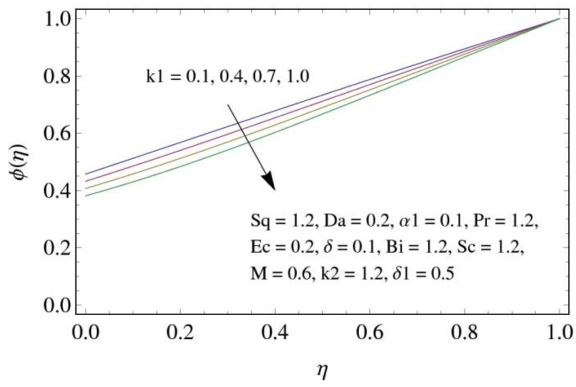

Fig. 15. (Color online) Variation of k_1 on $\phi(\eta)$.

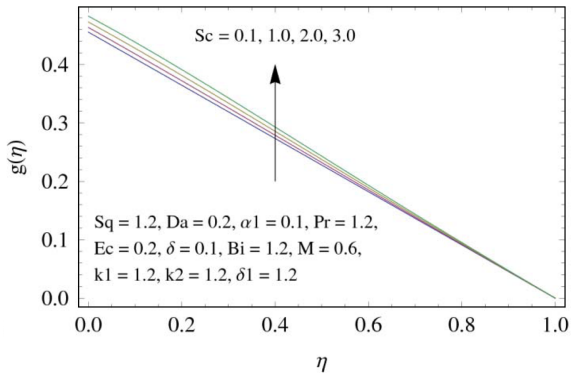

Fig. 16. (Color online) Variation of Sc on $g(\eta)$.

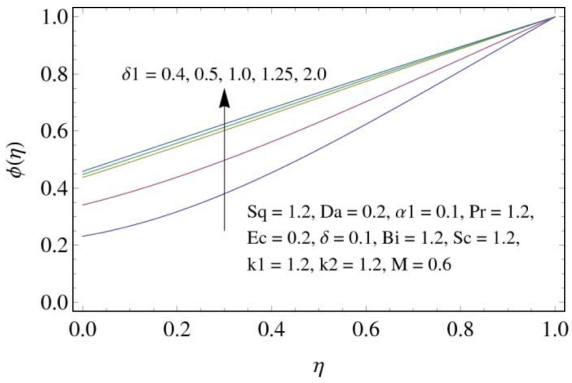

Fig. 17. (Color online) Variation of δ_1 on $\phi(\eta)$.

15 represents the behavior of strength of the heterogeneous reaction parameter k_1 on the concentration distribution. Hence larger estimation of k_1 leads to decays the concentration of the flow field because the reactants are consumed in the homogeneous reaction. Fig. 16 portrays the features of Schmidt number Sc on the concentration rate $g(\eta)$. An increment in Schmidt number causes to strengthen the concentration rate. As expected that higher Sc has larger mass diffusivity of concentration (b) of specie B which contributing rapid diffusion of mass. Hence the concentration rate $g(\eta)$ increases. Analysis of the ratio of the mass diffusion coefficient δ_1 on the concentration field of specie A is demonstrated in Fig. 17. It is found that concentration increases when δ_1 increases because mass diffusivity rises for increasing δ_1. In fact larger values of δ_1 strengthen the diffusion process inside the fluid. Hence concentration profile grows. Fig. 18 reflected the features of the ratio of mass diffusion coefficient δ_1 on concentration of specie B. It is noted that concentration distribution reduces for larger δ_1. Physically, larger vales of δ_1 yields lower mass diffusivity which leads to weak concentration distribution.

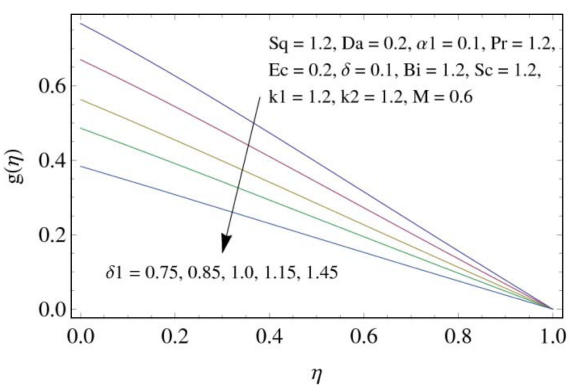

Fig. 18. (Color online) Variation of δ_1 on $g(\eta)$.

4.4. Skin friction coefficient and Nusselt number

Figure 19 reflects the variation of squeezing parameter S_q and magnetic parameter M on the skin friction co-efficient Cf. It is evident that skin friction co-efficient decays with increment in S_q whereas it enhances with M. Physically it justified that larger S_q provides more momentum transfer to the working fluid due to squeezing force and as the result the Cf decreases. Moreover, the magnetic parameter M depends on Lorentz forces (resistive

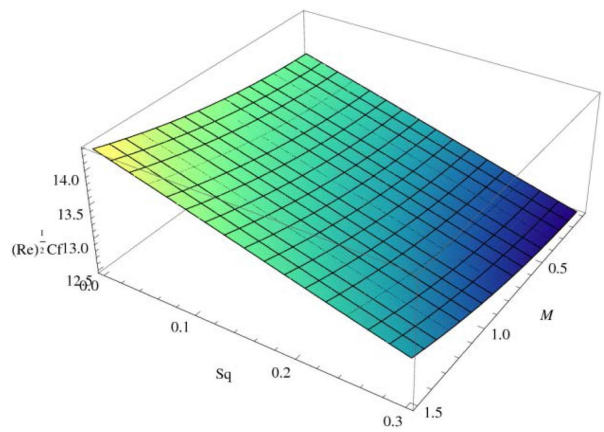

Fig. 19. (Color online) 3D plot of Cf with S_q & M.

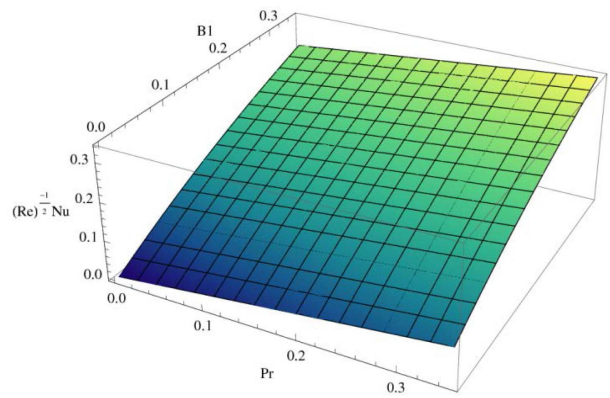

Fig. 20. (Color online) 3D plot of Nu with Pr & B_i.

force) which enhance the viscous forces and consequently skin friction co-efficient increases. Influence of Pr and B_i on Nusselt number is reflected in Fig. 20. It is noted that Nusselt number enhances with an increment in Prandtl number Pr and Biot number B_i. In fact enlargement in Pr results enhancement in thermal conductivity which is responsible for more heat transfer. Hence Nusselt number enhances. Further, Nusselt number is analyzed to increase for larger values of B_i which results due to sturdy thermal convection.

5. Closing Remarks

MHD squeezing flow of viscous fluid incorporates with viscous dissipation, Joule heating and homogeneous-heterogeneous reactions through non-Darcy porous medium are demonstrated. The conclusions drawn as follows:

- Larger magnetic parameter, Eckert and Biot numbers strengthen the temperature field.
- Dominant values of strength of homogeneous-heterogeneous reaction parameters are responsible for lower temperature field.
- Concentration of species A and B show opposite flow behavior for larger ratio of mass diffusion coefficient.
- Higher Schmidt number (Sc) depicts a lower concentration distribution (a) for specie A whereas concentration (b) of specie B shows increasing trend for larger.

References

[1] T. Hayat, A. Shafiq, M. A. Farooq, H. H. Alsulami, and S. A. Shehzad, J. Appl. Fluid. Mech. **9**, 1969 (2016).
[2] A. Hussain, M. Y. Malik, T. Salahuddin, S. Bilal, and M. Awais, J. Mol. Liq. **231**, 341 (2017).
[3] C. Sulochana, S. P. Samrat, and N. Sandeep, Int. J. Mech. Sci. **128**, 326 (2017).
[4] Z. A. Zaidi and S. T. Mohyuddin, J. Mol. Liq. **230**, 230 (2017).
[5] T. Hayat, Quratulain, A. Alsaedi, M. Rafiq, and B. Ahmed, Res. Phys. **6**, 1088 (2016).
[6] Y. Shagaiy, Z. A. Aziz, Z. Ismail, and F. Salah, Chin. J. Phys. **55**, 630 (2017).
[7] S. Das, R. N. Jana, and D. D. Makinde, Alex. Eng. J. **54**, 251 (2015).
[8] M. Waqas, M. I. Khan, T. Hayat, A. Alsaedi, and M. I. Khan, Euro. Phys. J. Plus **132**, 280 (2017).
[9] T. Hayat, M. I. Khan, A. Alsaedi, and M. I. Khan, Int. Comm. Heat. Mass. Trans. **89**, 190 (2017).
[10] Markin, Math. Comp. Mod. **24**, 125 (1996).
[11] T. Hayat, M. Farooq, and A. Alsaedi, J. Appl. Fluid. Mech. **9**, 809 (2016).
[12] M. I. Khan, T. Hayat, M. Waqas, M. I. Khan, and A. Alsaedi, J. Mol. Liq. **233**, 465 (2017).
[13] M. I. Khan, T. Hayat, M. I. Khan, and A. Alsaedi, Int. J. Heat. Mass. Trans. **113**, 310 (2017).
[14] H. Xu, Int. Comm. Heat. Mass. Trans. **87**, 112 (2017).
[15] T. Hayat, Z. Hussain, A. Alsaedi, and M. Mustafa, J. Tai. Inst. Chem. Eng. **70**, 119 (2017).
[16] M. Farooq and Aisha Anjum, J. Mol. Liq. **224**, 1341 (2016).
[17] C. S. K. Raju, N. Sandeep, and S. Saleem, Eng. Sci. Tech.: An Int. J. **19**, 875 (2016).
[18] M. I. Khan, M. Waqas, T. Hayat, M. I. Khan, and A. Alsaedi, J. Mol. Liq. **246**, 259 (2017).
[19] M. I. Khan, M. I. Khan, M. Waqasb, T. Hayat, and A. Alsaedi, Int. Comm. Heat. Mass. Trans. **86**, 231 (2017).
[20] Liao SJ. Beyond Perturbation: Introduction to Homotopy analysis method. Boca Raton: Chapman and Hall, CRC Press; 2003.
[21] Liao SJ. Homotopy Analysis Method in Non-linear differential equations. Heidelberg: Springer and Higher Education Press; 2012.
[22] T. Hayat, Hira Nazar, Maria Imtiaz, A. Alsaedi, and M. Ayub, Chin. J. Physi. **55**, 738 (2017).
[23] S. Abbasbandy, M. Yurusoy, and H. Gulluce, Math. Comp. Appl. **19**, 124 (2014).
[24] T. Hayat, M. Farooq, and A. Alsaedi, AIP Adv. **5**, 027130 (2015).
[25] J. Sui, L. Zheng, X. Zhang, and G. Chen, Int. J. Heat. Mass. Trans. **85**, 1023 (2015).
[26] M. I. Khan, M. Waqas, T. Hayat, and M. I. Khan, Int. J. Mech. Sci. **131**, 426 (2017).
[27] M. Waqas, M. I. Khan, T. Hayat, A. Alsaedi, and M. I. Khan, Chin. J. Phys. **55**, 729 (2017).
[28] T. Hayat, I. Ullah, A. Alsaedi, and M. Farooq, Results in Physics. **7**, 189 (2017).